Supporting Information for An Ovonic Threshold Switch Selector with Ultralow Threshold Voltage Drift Coefficient for Cross-Point Memory Applications

Xiaodan Li[1,2,3#], *Yuan Xue* [1,2#*], *Yuhao Wang* [1,2], *Tamihiro Gotoh* [4], *Sannian Song* [1,2]*, *Zhitang Song* [1,2]*

[1] National Key Laboratory of Materials for Integrated Circuits, Shanghai Institute of Microsystem and Information Technology, Chinese Academy of Sciences, 865 Changning Road, Shanghai 200050, China

[2] Center of Materials Science and Optoelectronics Engineering, University of Chinese Academy of Sciences, Beijing 100049, China

[3] Institute of Engineering Electronics China Academy of Engineering Physics, Mianyang 621999, China

[4] Department of Physics, Graduate School of Science and Technology, Gunma University, Maebashi 3718510, Japan

[5] Zhangjiang Laboratory

* Corresponding author. E-mail addresses: xueyuan@mail.sim.ac.cn, songsannian@mail.sim.ac.cn, ztsong@mail.sim.ac.cn

# These authors contributed equally to this work.

METHODS

Device Fabrication. The In-Te-As-Se-based OTS selector devices were fabricated in a TiN/In-Te-As-Se/TiN structure with a device area ranging from Φ200 nm to Φ60 nm to investigate the scalability of our devices. A 20 nm-thick In-Te-As-Se film was deposited from $In_{40}Te_{60}$ and $As_{40}Se_{60}$ targets using a co-sputtering technique in a Radiofrequency (RF) magnetron sputtering system. Then, the 40 nm-thick TiN films were deposited as a top electrode (TE) by employing the same sputtering technique. All devices were assembled at room temperature. The composition of the samples was determined as $In_5Te_9As_{30}Se_{56}$ (ITAS-1), $In_{8.5}Te_{15.5}As_{27}Se_{49}$ (ITAS-2), and $In_{16.8}Te_{27.4}As_{22.8}Se_{33}$ (ITAS-3). The effective device area is defined by that of the TiN bottom electrode (BE). Transmission electron microscopy (TEM) photos and the fast Fourier transform (FFT) patterns of this sample are shown in (Figure S1). The FFT pattern in area b clearly shows that the OTS layer is in an amorphous state. The energy dispersive spectroscopy (EDS) mapping in Figure S1b describes Ti, In, Te, As, and Se elements are evenly distributed.

Electrical Characterization. Electrical characterizations were conducted using a semiconductor parameter analyzer. Some series resistors were integrated with the OTS device as the current limiter. For this pulsed I-V measurement, a multi-channel oscilloscope has been used.

Band-structure Characterizations of Thin Films. Optical parameters and gap-state of In-Te-As-Se thin films were obtained from photothermal defection spectroscopy (PDS). The samples for PDS measurements were about 300 nm thick and deposited on fused quartz substrates. Excitation light for the PDS measurements came from a 100 W tungsten halogen lamp with a monochromator. The deflection signal was detected by a position-sensitive sensor. The samples were immersed in a liquid for the sake of signal enhancement. The valence band spectrum of the

films is determined by X-ray photoelectron spectroscopy (XPS). XPS measurement was performed by using monochromated Al K-Alpha ($h\nu = 1486.6$ eV) excited at 15 kV. The surfaces of the samples were etched and cleaned by Ar^+ (2 kV, 1 μA) for 60 s to remove oxides and contaminating impurities. Raman spectra data of 100 nm thick In-Te-As-Se films deposited on Si substrates were recorded using a Raman microscope (inVia Qontor) with an excitation wavelength of 633 nm.

Ab Initio Simulations. DFT-based ab initio molecular dynamics simulations (AIMD) were performed using the Vienna ab initio simulation package (VASP)[1]. The Perdew-Burke-Ernzerhof (PBE)[2] plane wave pseudopotential was used to describe the exchange-correlation function between electrons, and the projected enhanced wave (PAW) method[3] was used to describe the electron-ion interaction. A supercell containing 216 atoms (In:10, Te:19, As:66, Se:121 (ITAS-1), In:18, Te:34, As:58, Se:106 (ITAS-2), In:36, Te:59, As:49, Se:72 (ITAS-3), respectively, was constructed. First, the originally ordered unit cell structure was continuously insulated at 3000 K for 9 ps to melt to eliminate the initial crystal structure site, then the temperature was rapidly reduced to 1200 K within 30 ps seconds and then cooled to 300 K within 30 ps after holding at 1200 K for 30 ps, and the initial amorphous structure was obtained by relaxing at 300 K for 30 ps to achieve a steady state. Insulation relaxation during quenching is done to create zero residual stresses in the final amorphous structure. The MD time step was 3 fs, the plane wave energy cut-off was 400 eV, and the Brillouin zone was sampled at the Γ point. Apply Specification of Specification (NVT) ensembles and Nose-Hoover thermostats to control temperature and pressure during AIMD simulations.

To calculate the electronic structure, the amorphous model is fully relaxed at 0 K using the

conjugate-gradient method until the force on any atom is less than 0.01 eV/Å. The HSE06 hybrid functional was utilized to calculate the band gap of all amorphous models. The pseudopotential energy cut-off value is 400 eV, the energy converges to 1×10^{-6} eV, and the Γ point is selected for Brillouin zone sampling.

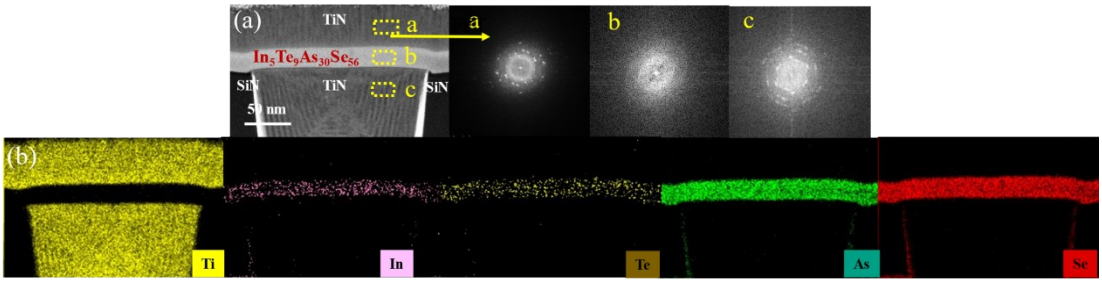

Figure S1. Cross-sectional TEM image of the TiN/InTeAsSe/TiN device. The deposition was performed in a vacuum process to prevent the oxidation of the chalcogenide film. subjected to several triangular pulses, and energy-dispersive spectroscopy (EDS) mappings of Ti, In, Te, As, and Se. The top and bottom electrodes are polycrystalline TiN, and the OTS material is amorphous and the elements are evenly distributed.

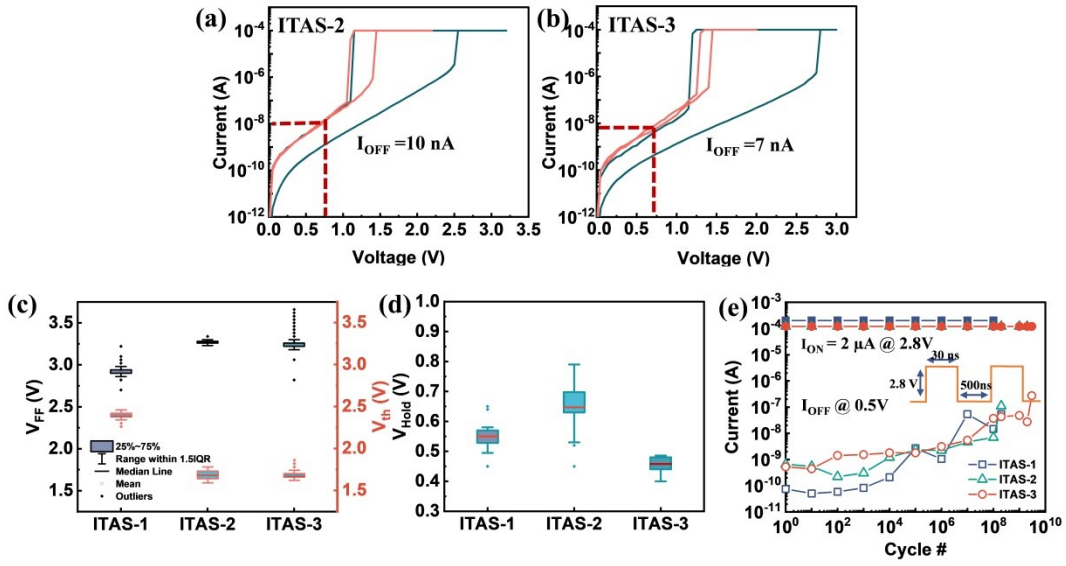

Figure S2. (a) Typical DC I-V characteristic of fabricated ITAS-2 OTS device. (b) Typical DC I-V characteristic of fabricated ITAS-3 OTS device. (c) and (d) V_{FF}, $V_{th,}$ and V_{hold} measured for all InTeAsSe OTS devices. (e) Endurance results for all InTeAsSe OTS devices. We applied a sequence of 10^9 pulses (rise time-width time-fall time equal to 20-30-20 ns). The ITAS-2 and 3 OTS devices have I_{OFF} values of 10 nA and 7 nA, respectively. The V_{FF} values for ITAS-1, ITAS-2, and 3 OTS are 2.94 V, 3.27 V, and 3.22 V, respectively. The corresponding V_{th} values are 2.38 V, 1.68 V, and 1.66 V, while the V_{hold} values are 0.55 V, 0.65 V, and 0.46 V, respectively.

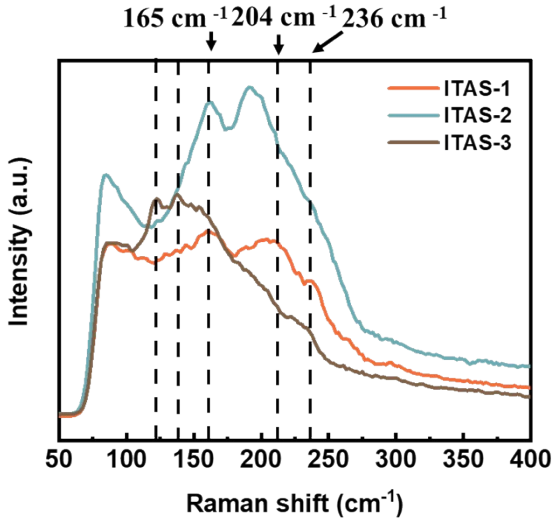

Figure S3. Comparison of Raman spectra of as-deposited ITAS-1, 2, and 3 thin films. The nature of the chemical bonds and the atomic environment of chalcogenide films are viewed through Raman analysis. The as-deposited ITAS-1 thin film has peaks at 165, 204, and 237 cm^{-1}, with the vibration of In-Se, $AsSe_{3/2}$ and $AsTe_3$[4], As_4Se_3 unit, respectively. The vibration of Se-Te is at a peak of 216 cm^{-1}[4]. The strong heteropolar bonds of In-Se and Se-Te are indeed formed in ITAS-1. Moreover, as the InTe content increases, we observed weakened peak intensities of 165 cm^{-1} and 204 cm^{-1} in ITAS-1 and ITAS-2, while a peak of 135 cm^{-1} emerged in ITAS-3, indicating an increase in the content of In-Te bonds. The peak position of 193 cm^{-1} in ITAS-2 may be a left shift of 204 cm^{-1}, which is related to the $AsTe_3$ structure unit. However, weak bonds can reduce

thermodynamic stability, resulting in a higher threshold voltage drift coefficient for ITAS-2 and 3 compared to ITAS-1.

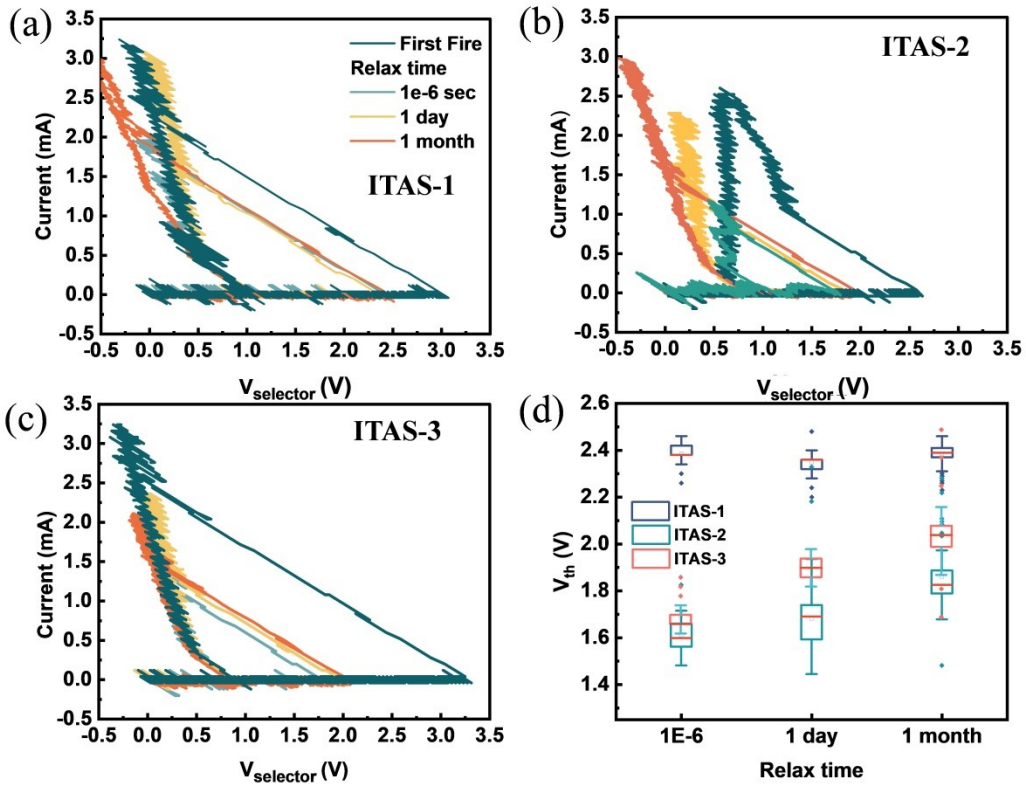

Figure S4. (a), (b) and (c) are typical pulsed-IV curves of ITAS-1, 2, and 3 OTS devices during relaxation measurement, respectively. (d) The V_{th} distribution of ITAS device cells is relaxed for 1 day and 1 month.

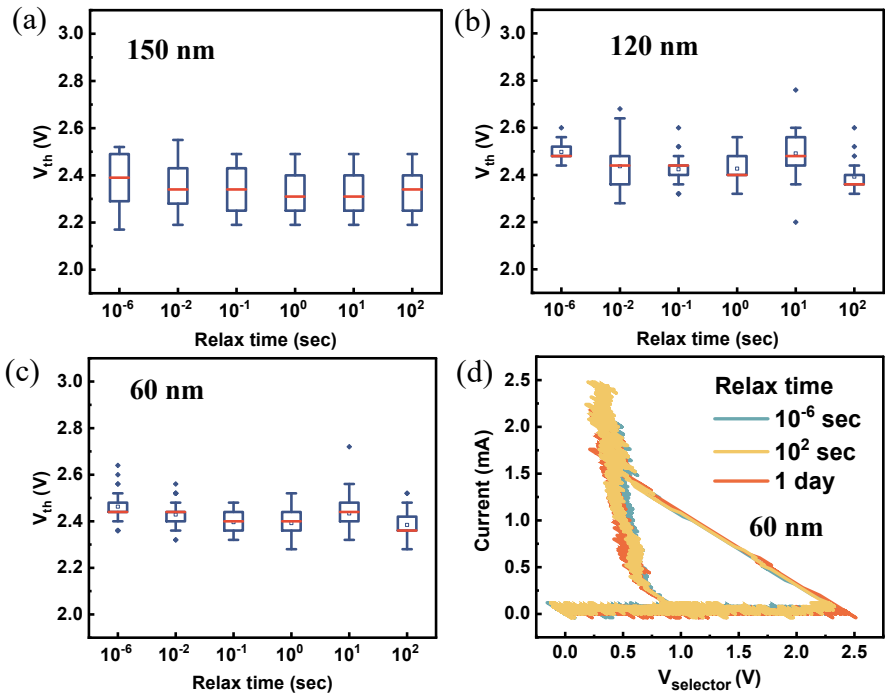

Figure S5. Measured V_{th} in the ITAS-1 devices with the relaxation time range from 1μs to 100 s with (a) BE 60, (b) 120, and (c) 150 nm. The pulse rising and falling time are 1μs. For more accurate analysis, the V_{th} of more than 50 cells was collected for each t_{relax}. (d) Typical pulsed-IV curves of ITAS-1 OTS device with BE 60 nm during relaxation measurement.

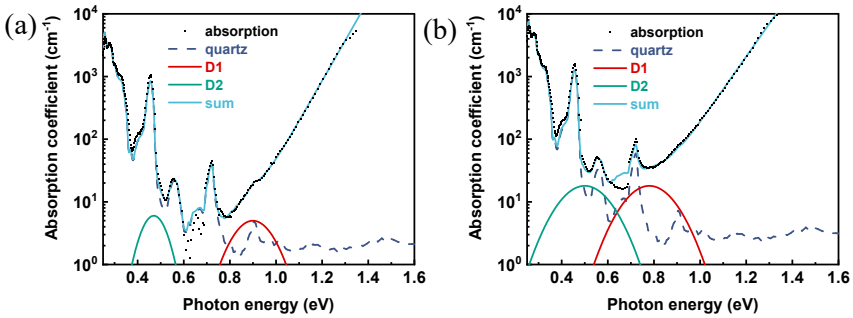

Figure S6. Photothermal deflection spectra (PDS) of as-deposited (a) ITAS-2 and (b) ITAS-3 film/quartz, and quartz substrate and calculation results based on Gaussian distribution.

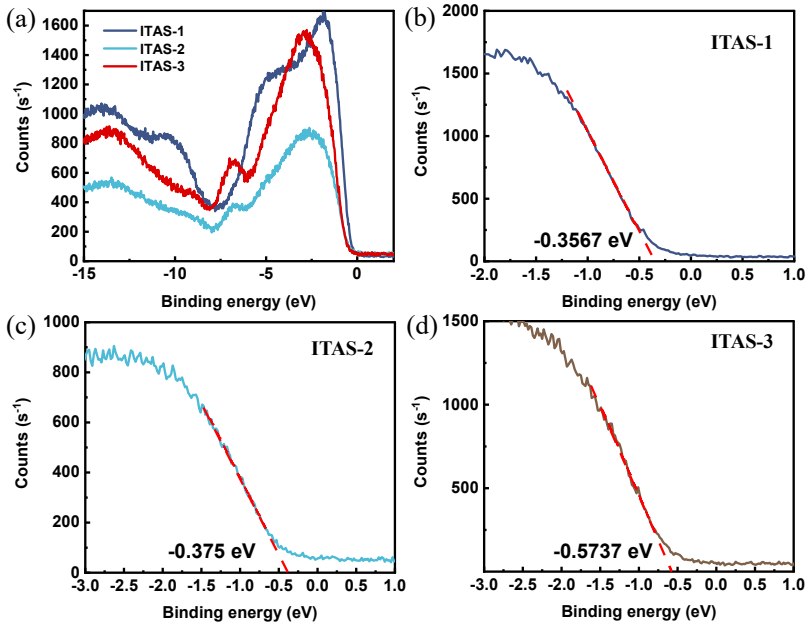

Figure S7. The Fermi levels of ITAS-1, 2, and 3 of the thin film are obtained by linear fitting after being corrected for the charge effect E_F of the carbon peak, and the Fermi levels of ITAS-1, 2, and 3 are 0.3567 eV, 0.375 eV, and 0.5737 eV, respectively.

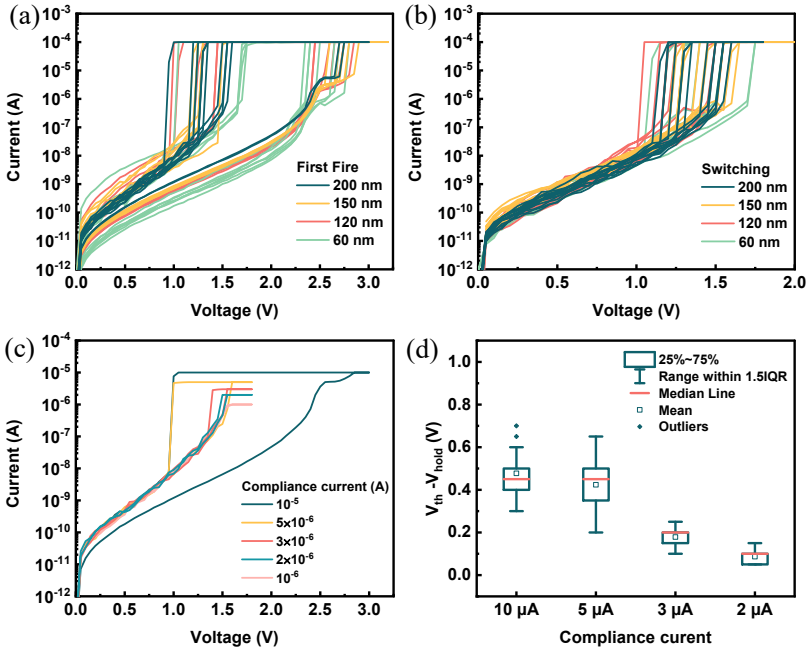

Figure S8. Leakage current (a) is area dependent at fresh-state before FF. (b) is area independent after FF. (c) DC I-V curves of the ITAS-1 OTS device with various compliance current I_{CC}. (d) V_{th}-V_{hold} as a function of I_{CC}. The leakage current decreases with the increase of the electrode size

during Forming, and the leakage current does not depend on the electrode size during subsequent switching. When the limiting current is smaller, the holding voltage is larger, which is similar to the conduction of conductive filaments in a conductive bridge gating tube. Explain that the OTS strobe is a conductive filament switching mechanism. As the current decreases, the smaller the diameter or number of conductive filaments formed, and V_{hold} cannot be kept at a lower value.

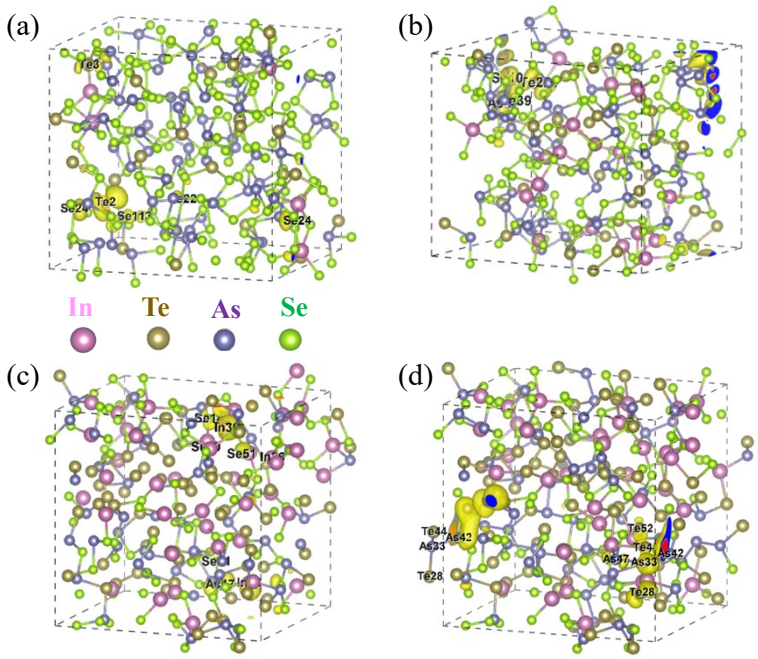

Figure S9. The sub-gap states are projected onto real space, in which the yellow regions represent the molecular-orbital charge density of the associated sub-gap states. (a) The trap D1 in the amorphous ITAS-1 film, (b) The trap D1 in the amorphous ITAS-2 film, (c) and (d) The trap D2 and D1 in the amorphous ITAS-3 film, respectively. The pink, brown, purple, and green balls represent In, Te, As, and Se atoms, respectively. The yellow isosurfaces, in both configurations, depict the molecular-orbital wavefunction amplitude of defect states and are plotted with isovalues of +0.0015 and −0.0015, respectively.

REFERENCES

1. G. Kresse and J. Hafner, *Physical review B*, 1993, **47**, 558.
2. J. P. Perdew, K. Burke and M. Ernzerhof, *Physical review letters*, 1996, **77**, 3865.

3. P. E. Blöchl, *Physical review B*, 1994, **50**, 17953.
4. R. Alekberov, S. Mekhtiyeva, G. Isayeva and A. Isayev, *Semiconductors*, 2014, **48**, 800-803.